NUMERICAL RECONSTRUCTION OF THE QUANTAL EVENT AT NICOTINIC SYNAPSES

JOHN C. WATHEY, MENASCHE M. NASS, AND HENRY A. LESTER, *Division of Biology, California Institute of Technology, Pasadena, California 91125 U.S.A.*

ABSTRACT To test our present quantitative knowledge of nicotinic transmission, we reconstruct the postsynaptic conductance change that results after a presynaptic nerve terminal liberates a quantum of acetylcholine (ACh) into the synaptic cleft. The theory assumes that ACh appears suddenly in the cleft and that its subsequent fate is determined by radial diffusion, by enzymatic hydrolysis, and by binding to receptors. Each receptor has one channel and two ACh binding sites; the channel opens when both sites are occupied and the rate-limiting step is the binding and dissociation of the second ACh molecule. The calculations reproduce the experimentally measured growth phase (200 μs), peak number of open channels (2,000), and exponential decay phase. The time constant of the decay phase exceeds the channel duration by $\simeq$20%. The normal event is highly localized: at the peak, two-thirds of the open channels are within an area of 0.15 μm^2. This represents 75% of the available channels within this area. The model also simulates voltage and temperature dependences and effects of inactivating esterase and receptors. The calculations show that in the absence of esterase, transmitter is buffered by binding to receptors and the postsynaptic response can be potentiated.

INTRODUCTION

Recent experiments provide quantitative data on several aspects of cholinergic transmission to muscle fibers and to electroplaques (reviewed by Gage, 1976; Steinbach and Stevens, 1976). To test the completeness of our knowledge, we have attempted to model the postsynaptic conductance change that results when the presynaptic terminal liberates a quantum of acetylcholine (ACh) into the synaptic cleft. The calculations were also undertaken to illuminate several questions, not yet subject to direct experiments, concerning the detailed spatial and temporal profile of receptor activation, esterase activity, and transmitter spread during the quantal event.

In our formulation, acetylcholine appears suddenly in the synaptic cleft; and its subsequent fate is determined by diffusion in the plane of the synaptic cleft, by enzymatic hydrolysis, and by binding to receptors. Previous investigators studied special cases that allow for solutions by analytic methods (Gage, 1976) or by analog computers (Rosenberry, 1979); their results have begun to describe how these processes shape the quantal response. We sought to extend this picture to more general conditions and therefore employed numerical methods. Our work borrows heavily from earlier models (Eccles and Jaeger, 1958; Kordas, 1972*a*,*b*; Magleby and

---

Mr. Wathey's present address is: Department of Neurosciences, University of California, San Diego, La Jolla, Calif. 92093.

BIOPHYS. J. © Biophysical Society · 0006-3495/79/07/145/20 $1.00
Volume 27 July 1979 145–164

Stevens, 1972*a,b;* Steinbach and Stevens, 1976; Jakopin and Kordas, 1977; Matthews-Bellinger and Salpeter, 1978).

We have devoted particular attention to three important characteristics of the normal quantal response. First, the growth phase lasts ≃200 μs (Gage and McBurney, 1975; Lester et al., 1978). Second, 1,000–2,000 receptor channels are open at the peak of the quantal response (Katz and Miledi, 1972; Anderson and Stevens, 1973). Finally, the declining phase has an exponential time-course, and under appropriate conditions the time constant equals the average lifetime of open channels—typically, 0.5–10 ms. These characteristics are altered by various well-characterized pharmacological and electrophysiological manipulations; and in several cases our model simulates such effects.

THEORY

The Fundamental Assumptions

Tables I and II define the symbols used throughout this paper. Both sub- and superscripts will be used; letter superscripts do not denote powers.

GEOMETRY The synaptic cleft is represented as the space within the disc of height H and radius R, bounded at the top by the membrane of the nerve terminal and at the bottom by that of the postsynaptic cell. The radial coordinate r is the distance, measured parallel to the membranes, from the axis of this disc. The cleft is open to the external solution at the edge.

RELEASE MECHANISM Very little is known about the spatial and temporal details of transmitter release during a single quantal event. We simply assume that at time $t = 0$ all the transmitter in a quantium appears instantaneously in the synaptic cleft as a radially symmetric distribution (see Initial and Boundary Conditions, below).

The subsequent fate of ACh, in our calculations, is determined by three processes: diffusion, interaction with esterase, and interaction with receptors. Radially symmetric equations describe these processes. Furthermore, we remove the vertical coordinate by assuming that ACh mixes instantaneously along the height of the cleft.

$$\frac{\partial a(r,t)}{\partial t} = \frac{\partial a(r,t)}{\partial t}\Big]_{\text{diffusion}} + \frac{\partial a(r,t)}{\partial t}\Big]_{\text{esterase}} + \frac{\partial a(r,t)}{\partial t}\Big]_{\text{receptors.}} \tag{1}$$

For simplicity, we omit the (r, t) from equations below.

DIFFUSION We assume that Ach's diffusion coefficient does not depend on concentration. The diffusion term becomes, simply:

$$\frac{\partial a}{\partial t}\Big]_{\text{diffusion}} = D\left(\frac{\partial^2 a}{\partial r^2} + \frac{1}{r}\frac{\partial a}{\partial r}\right). \tag{1A}$$

INTERACTION WITH ESTERASE We assume that catalytic sites of acetylcholinesterase (E) are present at a uniform density, e_0. Acetylcholine (A) can bind to these sites and undergo hydrolysis. A simplified version of this scheme is:

$$\mathrm{A} + \mathrm{E} + \mathrm{H_2O} \xrightarrow{k_1} \mathrm{AE} \xrightarrow{k_3} \mathrm{E} + \text{acetate} + \text{choline} + \mathrm{H^+}. \tag{2}$$

Here AE represents several intermediate states that interconvert rapidly (Rosenberry, 1975)

and cannot bind additional ACh. Therefore,

$$\left.\frac{\partial a}{\partial t}\right]_{\text{esterase}} = -k_1(e_0 - e^{\wedge})a \tag{1B}$$

and

$$\frac{\partial e^{\wedge}}{\partial t} = k_1(e_0 - e^{\wedge})a - k_3 e^{\wedge}. \tag{3}$$

The density of ACh that has been removed by the esterase, a^h, is the sum of the esterase-bound and hydrolyzed ACh densities. One has:

$$\frac{\partial a^h}{\partial t} = -\left.\frac{\partial a}{\partial t}\right]_{\text{esterase}}. \tag{7}$$

INTERACTION WITH RECEPTORS We assume that receptors (R) are present at a density, c_0, in the postsynaptic membrane, and that they bind ACh reversibly. Each receptor has one channel and two binding sites for ACh. The channel opens if and only if both sites are occupied; and the rate-limiting step in channel opening and closing is the binding and dissociation of the second ACh molecule (see, for instance, Sheridan and Lester, 1977).

$$2\mathrm{A} + \mathrm{R} \underset{k_{-1}}{\overset{2k_{+1}}{\rightleftharpoons}} \mathrm{A} + \mathrm{AR} \underset{2k_{-2}}{\overset{k_{+2}}{\rightleftharpoons}} \mathrm{A_2R^*}. \tag{4}$$

The state A_2R^* has an open channel.

$$\left.\frac{\partial a}{\partial t}\right]_{\text{receptors}} = -2k_{+1}(c_0 - c^{\mathrm{I}} - c^{\mathrm{II}})a - k_{+2}c^{\mathrm{I}}a + k_{-1}c^{\mathrm{I}} + 2k_{-2}c^{\mathrm{II}} \tag{1C}$$

and

$$\frac{\partial c^{\mathrm{I}}}{\partial t} = 2k_{+1}(c_0 - c^{\mathrm{I}} - c^{\mathrm{II}})a + 2k_{-2}c^{\mathrm{II}} - k_{+2}c^{\mathrm{I}}a - k_{-1}c^{\mathrm{I}}; \tag{5A}$$

$$\frac{\partial c^{\mathrm{II}}}{\partial t} = k_{+2}c^{\mathrm{I}}a - 2k_{-2}c^{\mathrm{II}}, \tag{5B}$$

The density of ACh bound to receptors is:

$$a^b(r, t) = c^{\mathrm{I}}(r, t) + 2c^{\mathrm{II}}(r, t). \tag{6}$$

Initial and Boundary Conditions

ZERO TIME At $t = 0$ (the instant of quantal release) the densities $e^{\wedge}$, c^{I}, c^{II}, and a^h are zero everywhere: i.e., all esterase and receptor sites are free, all channels are closed, and no ACh has been hydrolyzed. We assume that the initial ACh density is:

$$a(r, 0) = \begin{cases} \alpha\left[\left(\frac{r}{V}\right)^4 - 2\left(\frac{r}{V}\right)^2 + 1\right] & \text{if } 0 \le r \le V \\ 0 & \text{if } r > V. \end{cases} \tag{8}$$

If the initial ACh density is contained within the radius of the synaptic vesicle, V becomes the "vesicle radius." Eq. 8 is used because it approximates a Gaussian distribution and because its spatial integral can be obtained analytically. The scaling factor α is calculated from V and from A_0, the number of molecules released:

$$\alpha = \frac{3A_0}{\pi V^2}. \tag{9}$$

EDGE OF THE CLEFT We assume that transmitter diffuses away rapidly when it reaches the edge of the cleft, that is,

$$a(R, t) = 0 \tag{10}$$

for all t. This condition forces the other density functions to zero at $r = R$ for all t.

Summary of Equations to be Solved

Radially symmetric functions are obtained by numerical integration of the coupled system of equations:

$$\frac{\partial a}{\partial t} = \frac{\partial a}{\partial t}\Big]_{\text{diffusion}} + \frac{\partial a}{\partial t}\Big]_{\text{esterase}} + \frac{\partial a}{\partial t}\Big]_{\text{receptors}}. \tag{1}$$

$$\frac{\partial a}{\partial t}\Big]_{\text{diffusion}} = D\left[\frac{\partial^2 a}{\partial r^2} + \frac{1}{r}\frac{\partial a}{\partial r}\right] \tag{1A}$$

$$\frac{\partial a}{\partial t}\Big]_{\text{esterase}} = -k_1(e_0 - e^A)a \tag{1B}$$

$$\frac{\partial a}{\partial t}\Big]_{\text{receptors}} = -2k_{+1}(c_0 - c^I - c^{II})a - k_{+2}c^I a + k_{-1}c^I + 2k_{-2}c^{II} \tag{1C}$$

$$\frac{\partial c^I}{\partial t} = 2k_{+1}(c_0 - c^I - c^{II})a + 2k_{-2}c^{II} - k_{+2}c^I a - k_{-1}c^I; \tag{5A}$$

$$\frac{\partial c^{II}}{\partial t} = k_{+2}c^I a - 2k_{-2}c^{II}, \tag{5B}$$

$$\frac{\partial e^A}{\partial t} = k_1(e_0 - e^A)a - k_3 e^A. \tag{3}$$

$$\frac{\partial a^h}{\partial t} = -\frac{\partial a}{\partial t}\Big]_{\text{esterase}}; \tag{7}$$

subject to the initial and boundary conditions, Eqs. 8–10.

These equations are solved to yield density functions of r and t, as in Fig. 2 below. It is often interesting to know the spatial integrals of these densities, as in Fig. 1 below. In particular, the important quantity,

$$C^{II}(t) = 2\pi \int_0^R c^{II}(r, t) r dr,$$

is the total number of receptor channels in the open state at time t. This function gives the waveform of the miniature postsynaptic current recorded with a focal external electrode or with a voltage-clamp circuit. The magnitude of the current is the product of C^{II}, the single-channel conductance, and the electrochemical driving force.

TABLE I
VARIABLES OF THE CALCULATION

Variables	Symbol	Unit
Independent		
Radius	r	μm
Time	t	ms
Dependent	*Density (per μm²)*	*Spatial integral*
Free ACh	$a(r,t)$	$A(t)$
Bound acetylcholinesterase sites (AE)	$e^{\wedge}(r,t)$	$E^{\wedge}(t)$
ACh eliminated by esterase	$a^{h}(r,t)$	$A^{h}(t)$
Singly bound receptors (AR)	$c^{I}(r,t)$	$C^{I}(t)$
Doubly bound receptors (A_2R^*)	$c^{II}(r,t)$	$C^{II}(t)$
ACh bound to receptors	$a^{b}(r,t)$	$A^{b}(t)$
ACh diffused from cleft*	—	$A^{d}(t)$

*Calculated from $A^{d}(t) = A_0 - A(t) - A^{h}(t) - A^{b}(t)$.

NUMERICAL METHODS

We used a "mini" computer (Nova 2, Data General Corp., Westboro, Mass.) equipped with 32K core storage and software multiply/divide. The program is written in BASIC with simple extensions to allow X-Y plotting through digital-to-analog converters. The program runs under the Diskette Operating System.

Notation

Let $f(r, t)$ represent any of the densities (Table I), and let $F(t)$ represent the spatial integral of $f(r, t)$. If δr and δt are radial and time increments respectively, then we define:

$$r_i = i\delta r, \qquad (i = 0, 1, 2, \ldots, N)$$

$$t_j = \Sigma_j \delta t_j,$$

$$f_{i,j} = f(r_i, t_j),$$

and

$$F_j = F(t_j).$$

The integers i and j are the radial and temporal indices, respectively, and N is the total number of radial intervals. The time increment from t_j to t_{j+1} is δt_j. (Because the time increments are often changed, $t_j \neq j\delta t$.) For each time index, j, the radial density array is the collection of values $f_{i,j}$ where $i = 0, 1, \ldots, N$.

Strategy

The densities are calculated as radial arrays for each time value. At $t = 0$ (i.e., $j = 0$) the initial conditions specify all five radial density arrays. Finite difference methods are used to extrapolate new sets of radial density arrays at $t_1 = \delta t_0$, $t_2 = \delta t_0 + \delta t_1$, etc. In the discussion that follows, the index "j" denotes a known array or array element (i.e., at time t_j); the index "$j+1$" denotes an unknown (to be calculated) array or array element; for simplicity we usually omit the subscript from δt_j.

Computing the Radial Density and Spatially Integrated Arrays

The steps in the computation of the arrays $f(r,t)$ and $F(t)$ are summarized by the sequence: (a) set initial conditions and initial δt; (b) calculate spatial integrals of radial density arrays to obtain A_j, A^{h}_j, C^{I}_j, C^{II}_j, and $E^{\wedge}_j$; (c) extrapolate tentative values for $c^{I}_{i,j+1}$, $c^{II}_{i,j+1}$, and $e^{\wedge}_{i,j+1}$, $i = 0, \ldots, N-1$; (d) solve for

$a_{i,j+1}$, $i = 0, \ldots, N-1$, using known densities $f_{i,j}$ and values calculated in (c); (e) if necessary, change δr and repeat (c) and (d); (f) using $a_{i,j}$ and $a_{i,j+1}$, calculate $a^h_{i,j+1}$ and corrected values for $c^{\mathrm{I}}_{i,j+1}$, $c^{\mathrm{II}}_{i,j+1}$, and $e^{\mathrm{A}}_{i,j+1}$, for all $i = 0, \ldots, N-1$; (g) increase t by δt, test δt, and change if necessary; (h) repeat (starting with step b) for the next time step.

We now provide details of these steps and discuss the accuracy of the solution.

Spatial Integration of the Radial Density Arrays.

F_j is calculated as the volume under the surface of revolution defined by $f_{i,j}$. For each odd-indexed radius r_i, a parabola is fit to $f_{i-1,j}$, $f_{i,j}$, and $f_{i+1,j}$; the theorem of Pappus is used to compute the incremental volume.

Solving for a

An implicit finite difference approximation to Eq. 1 is used to extrapolate $a_{i,j+1}$ from $a_{i,j}$ (Crank, 1975; Smith, 1965). The diffusion, receptor, and esterase terms are replaced by weighted averages of their finite difference approximations at the j^{th} and $j+1^{\text{st}}$ time points:

$$\frac{a_{i,j+1} - a_{i,j}}{\delta t} = (1-\theta)(X_{i,j} + Y_{i,j} + Z_{i,j}) + \theta(X_{i,j+1} + Y_{i,j+1} + Z_{i,j+1}), \tag{11}$$

where θ is the weighting factor, and $X_{i,j}$, $Y_{i,j}$, and $Z_{i,j}$ are approximations at r_i and t_j to the diffusion, receptor, and esterase terms, respectively.

$$X_{i,j} = \begin{cases} \dfrac{D}{2i(\delta r)^2}\left[(2i+1)a_{i+1,j} - 4ia_{i,j} + (2i-1)a_{i-1,j}\right] & \text{if } i > 0; \\ \dfrac{4D}{(\delta r)^2}(a_{1,j} - a_{0,j}) & \text{if } i = 0; \end{cases} \tag{12}$$

$$Y_{i,j} = -2k_{+1}(c_0 - c^{\mathrm{I}}_{i,j} - c^{\mathrm{II}}_{i,j})a_{i,j} - k_{+2}c^{\mathrm{I}}_{i,j}a_{i,j} + k_{-1}c^{\mathrm{I}}_{i,j} + 2k_{-2}c^{\mathrm{II}}_{i,j}; \tag{13}$$

$$Z_{i,j} = -k_1(e_0 - e^{\mathrm{A}}_{i,j})a_{i,j}. \tag{14}$$

We find that θ must exceed somewhat the theoretical value of one-half to assure stability (Smith, 1965), probably because of the numerous changes made in δt and δr throughout a calculation. For most calculations, the value $\theta = 0.7$ served well. Eqs. 11–14 relate unknown densities at time t_{j+1} to their known values at t_j. For c^{I}, c^{II}, and e^{A}, unknown densities are tentatively extrapolated from their known values by using a first-order Runge-Kutta method (step c of algorithm):

$$f_{i,j+1} = \frac{\partial(f_{i,j})}{\partial t} \cdot \delta t + f_{i,j}. \tag{15}$$

At each radius $r_{i,j+1}$, the remaining unknowns are $a_{i-1,j+1}$, $a_{i,j+1}$, and $a_{i+1,j+1}$. As i takes on all values from 0 to $N-1$, Eq. 11 generates a system of N equations in N unknowns. This is solved (using Gauss' elimination method) to calculate the new radial array for a at t_{j+1} (step d).

Solving for c^{I}, c^{II}, e^{A}, and a^h

After step e, the ACh radial density arrays ($a_{i,j}$ and $a_{i,j+1}$) are known. These values are then used to extrapolate a^h and to correct the values of c^{I}, c^{II}, and e^{A} calculated from Eq. 15. The coupled system of Eqs. 5A and B is solved by assuming that $a = (a_{i,j} + a_{i,j+1})/2$ over the time interval $[t_j, t_{j+1}]$.

$$\begin{aligned} c^{\mathrm{I}}_{i,j+1} &= [\xi^{+}_{i,j+1}(\lambda_+ - m_4) + \xi^{-}_{i,j+1}(\lambda_- - m_4)]/m_3 \\ c^{\mathrm{II}}_{i,j+1} &= \xi^{+}_{i,j+1} + \xi^{-}_{i,j+1}, \end{aligned} \tag{16}$$

where:

$$\xi^{\pm}_{i,j+1} = \pm \left\{ \left[\frac{c^{I}_{i,j} m_3 + c^{II}_{i,j}(m_4 - \lambda_{\mp})}{\lambda_+ - \lambda_-} + \frac{\beta}{\lambda_\pm} \right] \exp(\lambda_\pm \delta t) - \frac{\beta}{\lambda_\pm} \right\}$$

$$\lambda_\pm = \tfrac{1}{2}\{m_1 + m_4 \pm [(m_1 + m_4)^2 - 4(m_1 m_4 - m_2 m_3)]^{1/2}\}$$

$$\beta = 2k_{+2}k_{+1}a^2 c_0/(\lambda_+ - \lambda_-),$$

and

$$m_1 = (-2k_{+1} - k_{+2})a - k_{-1}; m_2 = 2(k_{-2} - k_{+1}a); m_3 = k_{+2}a; m_4 = -2k_{-2}.$$

To solve Eq. 3 we assume that a varies linearly over $[t_j, t_{j+1}]$. Then:

$$e^{\wedge}_{i,j+1} = e_0 + \exp[-\beta_1(\delta t + \beta_2)^2] \cdot \left\{ (e^{\wedge}_{i,j} - e_0) \exp(\beta_1 \beta_2^2) - k_3 e_0 \int_0^{\delta t} \exp[\beta_1 (t + \beta_2)^2] \, dt \right\}, \quad (17)$$

where:

$$\beta_1 = k_1(a_{i,j+1} - a_{i,j})/2\delta t,$$

and

$$\beta_2 = (k_1 a_{i,j} + k_3)/2\beta_1.$$

The definite integral remaining in Eq. 17 is evaluated by Simpson's method.

Eq. 7 may now be integrated directly, assuming linear variation of both a and $e^{\wedge}$ over the time interval. The solution is:

$$a^{h}_{i,j+1} = a^{h}_{i,j} + \frac{k_1 \delta t}{2} [(e_0 - e^{\wedge}_{i,j})(a_{i,j} + a_{i,j+1}) + \frac{1}{3}(e^{\wedge}_{i,j} - e^{\wedge}_{i,j+1})(a_{i,j} + 2a_{i,j+1})], \quad (18)$$

which completes step f. The methods presented above (Eqs. 16–18) are used because the computer's limited storage capacity precludes the use of predictor-corrector methods.

Selection of δr

Radial accuracy is governed primarily by the fixed parameter N, the number of radial intervals. This number is constant during a calculation, but δr changes to satisfy the following considerations. The radial densities of interest are highly localized at early times (e.g., $V = R/20$ for the standard event), necessitating a small value for δr ($\simeq$1 nm). But the densities spread by roughly an order of magnitude as ACh diffuses, allowing larger values of δr at later times without loss of accuracy ($\delta r \simeq 10$ nm during the decay phase).

The following procedure is used to choose the appropriate δr. The calculations begin with a temporary boundary radius $R' = 2V$; the radial increment is $\delta r = R'/N$. At step e for each time point, R' and δr are increased if a significant amount of ACh has diffused nearly to R'. Let n equal the integer part of 0.95 N. Then, if $a_{n,j+1} > a_{0,j}/1{,}000$, R' and δr are doubled. The new radial arrays are filled with the even-indexed elements from the previous arrays and with zeroes at radii greater than the previous value of R'. This doubling continues until the new value of R' would exceed the cleft radius R. At this point, R' is permanently set to R, δr is increased proportionally, and the new radial arrays are constructed using a linear interpolation procedure.

Selection of δt

Similar considerations dictate the use of small values for δt initially ($\simeq$1 ns) and allow stepwise increases with no loss of accuracy (to 0.2 ms near the end of the decay phase). For each time point at step g,

fractional changes in a, c^{I}, and c^{II} are tested and compared with a fixed parameter Q_t ($0 < Q_t < 1$). If any of the following conditions are met, δt is too large and will be halved before computation continues; if none are met when 2 δt is tested, δt is doubled: (1) $a_{i,j+1} < (1 - Q_t)a_{i,j}$; (2) $\partial c^{I}_{i,j}/\partial t > 0$ and $(c^{I}_{i,j+1} - c^{I}_{i,j}) > Q_t(c_0 - c^{I}_{i,j})$; (3) $\partial c^{I}_{i,j}/\partial t < 0$ and $c^{I}_{i,j+1} < (1 - Q_t)c^{I}_{i,j}$; (4) and (5) are the analogs to (2) and (3), for c^{II}. The unknowns, $c^{I}_{i,j+1}$ and $c^{II}_{i,j+1}$, required for these tests are extrapolated using Eq. 15 and the δt being tested; the unknown $a_{i,j+1}$ is extrapolated using the tested δt and an explicit form of Eq. 11 with a second-order term,

$$a_{i,j+1} = a_{i,j} + \left(\delta t + \frac{(\delta t)^2}{2\delta t_{j-1}}\right)(X_{i,j} + Y_{i,j} + Z_{i,j}) + \frac{1}{2}\left(\frac{\delta t}{\delta t_{j-1}}\right)^2 (a_{i,j-1} - a_{i,j}).$$

Accuracy

Error estimates can be obtained by allowing N to grow very large and Q_t to approach zero; this forces the increments δr and δt to approach zero. We verified that the results converge to the same values as those obtained with slower, fully numerical (first- and second-order Runge-Kutta) solutions. For our algorithms, the $Q_t = 0.05$, $N = 180$ solution differs from the $Q_t = 0.1$, $N = 150$ solution by $< 0.5\%$ in all arrays. Therefore, the former solution is in error by $< 0.5\%$ in all the variables. However, this accuracy level requires 20 h to calculate a 3-ms simulation. We usually use $Q_t = 0.2$, $N = 50$; calculations require 1–2 h for most simulations and the error is $< 2\%$.

RESULTS

The "Standard" Quantal Event

ASSUMED PARAMETERS These are given in Table II, with appropriate references. The values have been selected or extrapolated to apply to frog muscle at a membrane potential of −85 mV and a temperature of 25°C (see Steinbach and Stevens, 1976). In the Discussion we comment further on these values. At this point, however, we note our arbitrary assumption that ACh diffuses in the synaptic cleft at a rate of 3×10^{-6} cm^2/s, or ⅓–½ its rate in free solution (Dreyer and Peper, 1974; Dionne, 1976). This assumption could well be an overestimate, because a diffusion constant of 10^{-6} cm^2/s characterizes several small aromatic amines in 8% gelatin at 25°C (Levenson, 1977). ACh's diffusion in the cleft could be slowed further by binding to hyaluronate groups of the basement membrane.

We also have little information on the rates that characterize the binding of the first ACh molecule to a receptor, $k_{\pm 1}$. Sheridan and Lester (1977) have given arguments for assuming that these rates exceed $k_{\pm 2}$ by at least fivefold, and we have adopted this lower limit. Of more importance for the calculations is the equilibrium constant for this step, $k_{-1}/2k_{+1}$. We have assumed that this equals 25 μM, or roughly the same as the equilibrium constant for the second binding ($2k_{-2}/k_{+2} = 33$ μM).

The cleft height, H, determines the constant of proportionality between the surface densities and volume densities. For the assumed standard value of 0.05 μm, 30,100 molecules/μm^2 corresponds to a concentration of 1 mM.

RADIALLY INTEGRATED TEMPORAL PLOTS The quantal event may be summarized by temporal plots of the total number of singly and doubly bound receptor molecules (Fig. 1*a*) and of transmitter molecules in all possible states (Fig. 1*b*). The computed evolution of open channels agrees well with the rather variable experimental voltage-clamp data on miniature postsynaptic currents. (a) The response rises to a peak in $\simeq$ 200 μs; the "growth time" (20–80% of peak) is 65 μs (Gage and McBurney, 1975; Lester et al., 1978). (b) At its peak,

TABLE II
ASSUMED PARAMETERS OF THE STANDARD QUANTAL EVENT

Parameter	Symbol	Value	References
Physical dimensions			
Vesicle radius	V	0.025 μm	Heuser and Reese, 1973; Peper et al., 1974
Cleft radius	R	0.5 μm	
Cleft height	H	0.05 μm	
Acetylcholine			
Molecules in a vesicle	A_0	10,000	Kuffler and Yoshikami, 1975; Fletcher and Forrester, 1975
Diffusion constant	D	3×10^{-6} cm^2/s	See text
Acetylcholinesterase			
Density*	e_0	2,600 sites/(μm)^2	Matthews-Bellinger and Salpeter, 1978
Forward binding rate	k_1	2×10^8 M^{-1}s^{-1}	Rosenberry, 1975
Turnover rate	k_3	1.6×10^4s^{-1}	Rosenberry, 1975
Receptors			
Density	c_0	12,000/(μm)^2	Matthews-Bellinger and Salpeter, 1978‡; J. E. Heuser§
First forward binding rate	$2k_{+1}$	3×10^8 M^{-1}s^{-1}	See text
First dissociation rate	k_{-1}	7.5×10^3 s^{-1}	See text
Second forward binding rate	k_{+2}	3×10^7 M^{-1}s^{-1}	Sheridan and Lester, 1977
Second dissociation rate	$2k_{-2}$	10^3s^{-1}	Sheridan and Lester, 1977; Steinbach and Stevens, 1976

*Value appropriate to mouse muscle.
‡Assuming two α-bungarotoxin sites per receptor channel.
§Density of membrane particles in rotary-shadowed freeze-fracture data.[2]

the quantal event involves ≃ 2,060 channels (Katz and Miledi, 1972; Anderson and Stevens, 1973). (c) The response decays exponentially with time; the rate constant (0.82 ms^{-1}; least-squares fit to the logarithm of the response) is close to that ($2k_{-2}$ = 1 ms^{-1}) for channel closing (Magleby and Stevens, 1972*a,b;* Anderson and Stevens, 1973; Neher and Sakmann, 1975; Sheridan and Lester, 1975, 1977).

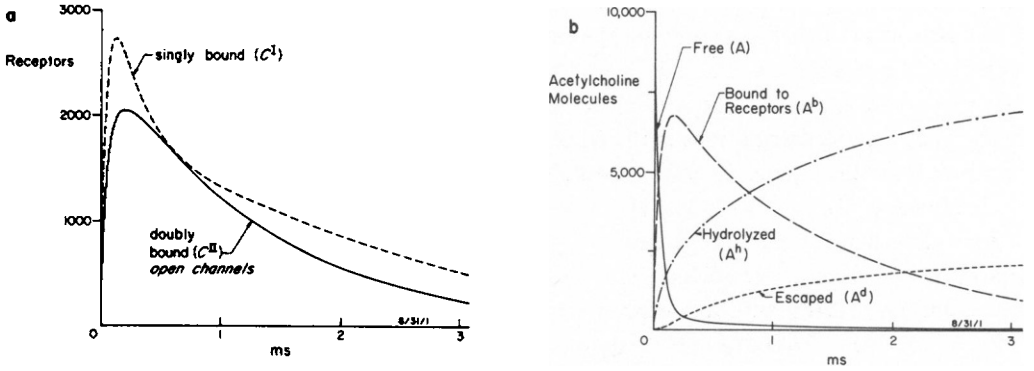

FIGURE 1 (*a*) Singly and doubly bound receptors during the standard quantal event; (*b*) fate of the 10,000 transmitter molecules released into the synaptic cleft at the beginning of the standard quantal event. Radially integrated temporal plots.

[2]Heuser, J. E. Personal communication.

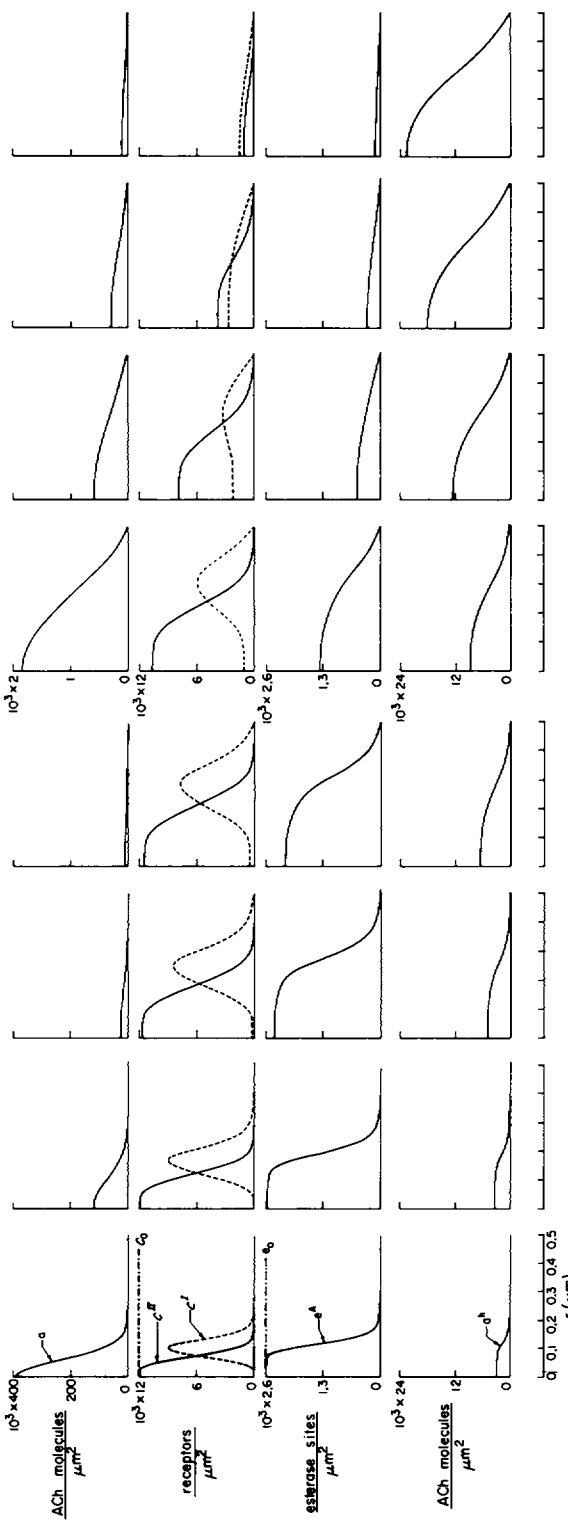

FIGURE 2 Isochronous radial plots for the standard event, at each indicated time.

Singly bound receptors have closed channels. Singly bound receptors are present in large numbers throughout the quantal event (Fig. 1*a*), usually outnumbering doubly bound receptors. As explained in greater detail below, the two populations have quite different spatial distributions.

By the time the response has reached its peak (207 μs), only 517 of the original 10,000 ACh molecules remain free in the synaptic cleft (Fig. 1*b*). This result agrees with the conjecture of Magleby and Stevens (1972*a*,*b*). An additional 484 molecules are bound to acetylcholinesterase (not shown). However, a much larger number (6,677 molecules) are bound to receptors, in agreement with the conclusions of Katz and Miledi (1973), Magleby and Terrar (1975), and Hartzell et al. (1975). This point is discussed in greater detail below.

At all times, enzymatic hydrolysis removes more transmitter from the cleft than does diffusional loss. The exact ratios depend on several of the parameters (see below), but for the "standard event" one may summarize with the statement that after 3 ms, 6,955 ACh molecules have been destroyed by hydrolysis; 2,083 have diffused away at the edge of the cleft; 932 are still bound to receptors; and a few dozen more are bound to esterase or free in the cleft.

ISOCHRONOUS RADIAL PLOTS Such plots provide the most detailed view of the calculated results (Fig. 2). The various densities change quite rapidly during the first 1 μs or so. During this time, events depend strongly on the parameters of the initial ACh distribution; we possess no relevant experimental data on this point. After the first 5 μs, similar radial plots result from all reasonable values for the initial distribution and we therefore start our description at 6 μs.

At the earliest times, singly bound receptors predominate over doubly bound receptors (open channels) at all radii, but doubly bound receptors increase rapidly and by 6 μs (Fig. 2*a*) the latter predominate up to a radius of 0.075 μm (encompassing only 212 total receptors). At all times the doubly bound receptors have their highest density at the point of release; but the distribution of singly bound receptors forms an annulus that broadens and travels outward radially. At radii > 0.3 μm there are always more singly than doubly bound receptors.

When the response is at its peak, ⅔ of the 2,057 open channels are located within 0.221 μm of the origin. Because this radius encompasses 1,841 total receptors, 74.5% of them are activated. When the response has declined to ½ its peak value (1.2 ms) a slightly larger radius—0.24 μm—contributes ⅔ of the response. Thus the calculations provide quantitative support for recent suggestions that (*a*) a quantum of ACh activates most receptors within a small area; and that (*b*) this small area accounts for most of the response (Hartzell et al., 1975; Fertuck and Salpeter, 1976; Lester et al., 1978; Matthews-Bellinger and Salpeter, 1978).

The maximal velocity of ACh hydrolysis is the enzyme density times the deacylation rate k_3, or 4.16×10^4 molecules/(ms · μm^2). This velocity is approached for ACh concentrations high enough to saturate the esterase binding sites. Such is the case at early times near the release point; indeed, the local ACh concentration is so high that only a small fraction of the transmitter molecules can be hydrolyzed before binding to receptors (Fertuck and Salpeter, 1976, 1978; Rosenberry, 1979). After ≃200 μs, the ACh concentration at the origin falls below the value for half-maximal velocity (k_3/k_1 = 80 μm = 2,400 molecules/μm^2); enzymatic removal is then best described as a first-order process with a rate constant equal to

the esterase density times the forward binding rate k_1, or 17.2 ms^{-1}. This low-concentration description applies throughout the quantal event at radii greater than approximately 0.3 μm.

Systematic Variation of the Parameters

To determine which assumptions critically affect the waveform and amplitude of the calculated quantal event, we have varied many of the parameters around their standard values (Table III). The computed quantal event may be characterized by the time to peak, growth time (20–80% of peak), peak channels activated, and decay rate constant. These characteristics vary little with some of the geometrical parameters, such as vesicle and cleft sizes and diffusion constants. This insensitivity may explain how quantitatively similar quantal events can be recorded at nerve-muscle and nerve-electroplaque synapses from many different vertebrates. Other parameters strongly influence the quantal event: the peak amplitude is nearly proportional to the number of molecules in a vesicle; and the decay rate constant is nearly equal to the rate constant for channel closing, $2k_{-2}$.

Simulation of Experimental Manipulations

RECEPTOR AND ESTERASE BLOCKADE Table III includes some entries that directly simulate experimental manipulations. For example, receptors are blocked by elapid α-toxins with very low reversibility; and this process may be simulated by reducing receptor density. As a result, the calculated quantal event merely decreases in amplitude, with nearly constant waveform, in agreement with experimental data on the α-toxins (Lester, 1970; Katz and Miledi, 1973). For values of the density near the standard value (12,000 receptors/μm^2), the amplitude changes by only 3% with a 10% change in receptor density; but the dependence becomes almost directly proportional when the quantal event has been reduced in amplitude by about twofold. These observations support the agreement between results from two separate experimental approaches to measuring the toxin-receptor association rate: (a) blockade of endplate potentials (Lester, 1972) and (b) direct binding of radiolabeled toxin (Patrick et al., 1972; Weber and Changeux, 1974).

When the standard parameters are used with the exception that the esterase terms are omitted, the decay phase is still indistinguishable from a single exponential beginning 0.5–1 ms after the peak (Fig. 5 below). The decay rate constant decreases by nearly twofold and no longer approximates the channel closing rate (Table III). On the other hand, the growth phase is not much slower than for the standard event, and the peak is only 27% larger. These observations agree with recent voltage-clamp studies on effects of anticholinesterase drugs (Gage and McBurney, 1975). The quantal event spreads in the absence of esterase. At the peak of the response two-thirds of the open channels occur within an area of 0.21 μm^2 (vs. 0.15 μm^2 if the esterase is active). When the response has declined to half its peak value, the corresponding area is 0.25 μm^2 (vs. 0.18 μm^2 if the esterase is active).

BUFFERED DIFFUSION When neither hydrolysis nor binding to receptors is present, ACh molecules leave the cleft by diffusion alone. 1 ms after release only 0.013% of the ACh molecules remain in the cleft (see also Eccles and Jaeger, 1958). In contrast, when the esterase terms are omitted but the standard receptor binding is included, 65% of the molecules remain. In the latter calculations it is clear that (a) transmitter leaves the cleft slowly because

TABLE III
CHARACTERISTICS OF THE COMPUTED QUANTAL EVENT

	Growth time	Time to peak	Peak channels	Decay rate	Identifier
	μs	μs		ms^{-1}	
Standard event	65	207	2,057	0.82	6/21/3
	Systematic Variations of the Parameters				
Physical dimensions					
Vesicle radius, standard value, 25 nm					
2.5	65	205	2,057	0.83	6/24/5
250	56	195	2,052	0.83	6/24/2
Cleft radius, 0.5 μm					
0.25	31	105	1,272	0.93	1/26/2
0.375	57	175	1,928	0.86	1/27/1
10^4	65	210	2,062	0.79	6/24/3
Cleft height, 50 nm					
25	58	180	2,460	0.78	6/18/1
100	75	240	1,570	0.89	6/18/3
Acetylcholine					
Molecules in a vesicle, 10,000					
5,000	46	180	895	0.86	6/18/4
20,000	87	245	4,184	0.82	6/18/2
Diffusion constant, 0.3 $\mu m^2/ms$					
0.01	421	1,010	1,557	0.71	6/17/3
0.1	119	335	2,185	0.76	6/17/1
0.2	81	250	2,151	0.79	6/15/5
0.4	55	185	1,954	0.85	6/15/4
0.6	44	165	1,756	0.89	6/15/3
0.8	37	145	1,586	0.92	6/15/2
1.0	32	140	1,443	0.94	6/15/1
10.0		<12	197		6/17/4
Acetylcholinesterase					
Density, 2,600 sites/μm^2					
0	85	322	2,609	0.48	6/13/2
7,800	45	140	1,536	0.96	8/11/1
0, 1,200 receptors/μm^2	99	290	494	0.96	6/13/3
Receptors					
Density, 12,000/μm^2					
300	86	220	104	1.0	8/12/2
1,200	87	230	392	1.0	6/14/1
3,600	84	230	1,020	0.97	8/12/3
7,200	78	225	1,626	0.92	8/13/1
20,000	49	185	2,402	0.68	10/6/1
Channel closing rate, $2k_{-2}$ = 1 ms^{-1}					
0.25	78	335	2,257	0.23	6/19/4
0.5	72	265	2,170	0.44	6/19/2
2	57	170	1,901	1.48	6/19/1
4	49	135	1,969	2.3	6/19/3

it is buffered by rebinding to receptors, and that (b) this buffering effect tends to lengthen the calculated quantal event.

If, on the other hand, the calculations are performed with only 1/10 of the standard receptor density, an acetylcholine molecule is much more likely to diffuse out of the cleft than to bind

to one of the few receptors. The cleft soon contains too few transmitter molecules to produce an appreciable number of doubly bound channels; almost no channels open after the peak. Therefore, the decay phase has a time constant nearly equal to the channel duration, whether or not the esterase terms are included (Table III). These observations agree with experimental data on the combined effects of receptor and esterase blockade. Thus the model generates waveforms that are consistent with experimental data and support the conclusion that, in the absence of the esterase, transmitter molecules leave the cleft slowy because they bind repeatedly to receptors (Katz and Miledi, 1973; Magleby and Terrar, 1975; Armstrong and Lester, 1979).

VOLTAGE SENSITIVITY Endplate currents have a voltage-sensitive time-course, probably because voltage governs a rate-limiting step in the closing of the ACh-receptor channel (Magleby and Stevens, 1972*a,b;* Kordas, 1972*a,b*). To simulate the effect of changing voltage, we have varied $2k_{-2}$, the rate constant both for dissociation of one agonist molecule and for channel closing (Eq. 4). (We have assumed that k_{-1}/k_{+1} is not voltage-sensitive. However, the experimental data are not clear on this point. Sheridan and Lester [1977] were able to model their voltage-jump relaxations using this assumption; but the data can be fit almost as well by assuming that k_{-1}/k_{+1} is as voltage-sensitive as k_{-2}/k_{+2} [Lester et al., 1978].[1]) An *e*-fold increase in $2k_{-2}$ corresponds roughly to a shift of membrane potential by 85 mV in the positive direction (Magleby and Stevens, 1972 *a,b;* Gage and McBurney, 1975; Sheridan and Lester, 1975, 1977). Over the range from $2k_{-2} = 0.25$ ms^{-1} to 2 ms^{-1}—corresponding to a range of 177 mV—the peak activation varies by < 20%, but the decay rate constant changes by a factor of 6.43—almost as much as the channel duration (Table III and Fig. 3). Thus our calculations support the conjecture that the decay rate of the postsynaptic current is governed principally by the agonist-receptor interaction (Magleby and Stevens, 1972*a,b;* Kordas 1972*a,b*).

It is a clear experimental result that the decay rate retains most or all of its voltage sensitivity in the absence of acetylcholinesterase, although the rates themselves decrease by severalfold (Magleby and Stevens, 1972*a,b;* Kordas, 1972*a,b;* Gage and McBurney, 1975; Sheridan and Lester, 1977). With hyperpolarization the channel lifetime increases and transmitter remains bound to the receptor for a longer average time. Thus, the overall affinity of ACh for the receptor increases (Eq. 4), and transmitter is more strongly buffered by receptors. Therefore, the transmitter leaves the cleft more slowly and the decay is lengthened in a voltage-dependent fashion (Colquhoun, 1975; Lester et al., 1978). The calculations reproduce this effect (Fig. 3).

The experimental data are unclear about two, more subtle, calculated effects of variations in channel duration. The first point concerns the situation at very brief channel durations. For $2k_{-2} = 4$ ms^{-1}—corresponding to a membrane potential of +40 mV—the calculated quantal event does decay much more slowly than the channel duration, and the amplitude decreases. The experimental data are mixed on this point (Anderson and Stevens, 1973; Sheridan and Lester, 1977; Stevens, 1978). The second point is that the calculated growth phase becomes slightly faster as the channel duration decreases (Table II). Magleby and Stevens (1972*a,b*) noted that depolarization decreases the growth time of endplate currents, which are slightly

[1]Lester, H. A., D. D. Koblin, and R. E. Sheridan. Unpublished calculations.

asynchronous linear sums of quantal currents. In this laboratory, we have noted a similar effect in *Electrophorus* postsynaptic currents. Magleby and Stevens (1972*b*) attributed this result to voltage sensitivity of the opening rate but this interpretation rested on the assumption, now recognized as incorrect, that only a small proportion of receptors are activated during nicotinic transmission. Gage and McBurney (1975) found no significant voltage effects on the growth time of miniature endplate currents, but changes of the size predicted would probably have escaped notice.

TEMPERATURE The standard event is calculated with parameters appropriate to 25°C. We have simulated temperature variations by assuming that a Q_{10} of 1.25 applies to the diffusion coefficient for ACh and that the acetylcholinesterase binding rate, its turnover number, and the 4 receptor rate constants ($k_{\pm 1}$, $k_{\pm 2}$) all have a Q_{10} of 3. At 15°C the calculated growth time increases by a factor of 1.83; this could represent a significant discrepancy with the experimental measurement of 1.2 (Gage and McBurney, 1975).

Two other calculated effects of temperature agree well with the experimental data. (a) If the experimental Q_{10} of 1.5 for the amplitude of miniature postsynaptic currents (Gage and McBurney, 1975) is divided by an assumed value of 1.25 for the channel conductance, one concludes that actual quantal events involve 1.2 times fewer channels at 15 than at 25°C. In the simulations for 15°C, the calculated peak number of open channels decreases by a factor of 1.25. (b) At 15°C the calculated decay rate decreases by a factor of 2.73, which falls within the range of 2.5–3.5 measured experimentally in several laboratories (Gage, 1976; Steinbach and Stevens, 1976).

The experimental data are unclear on whether the rate constant for channel closing, $2k_{-2}$, has the same temperature sensitivity at all voltages (Anderson and Stevens, 1973; Gage and Van Helden, 1979). We have assumed that $2k_{-2}$ does have a voltage-independent Q_{10} of exactly 3. Nonetheless the calculated responses display a small interaction between temperature and the voltage dependence of the PSC decay rate. At −204 mV, the calculated decay

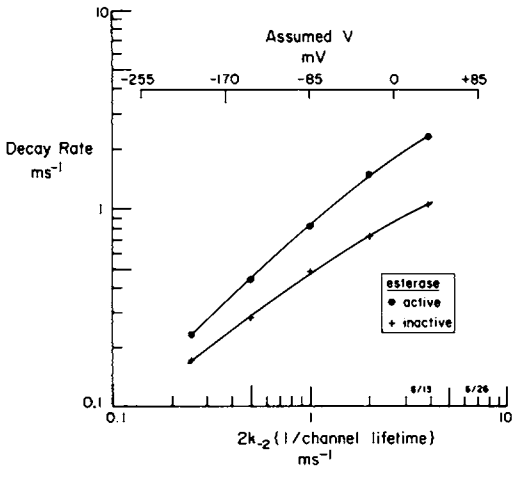

FIGURE 3

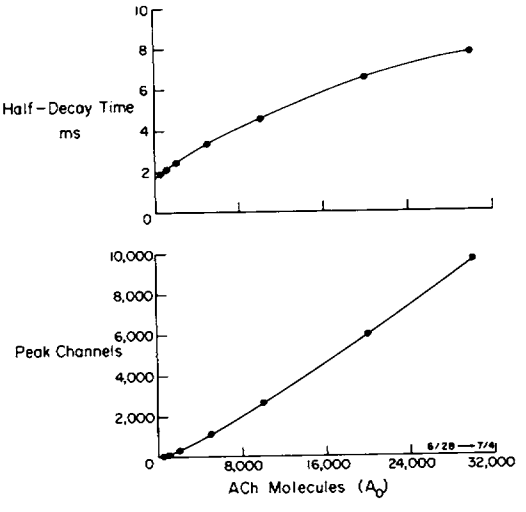

FIGURE 4

FIGURE 3 Voltage sensitivity of the calculated decay rate constant with and without esterase. See text.
FIGURE 4 Postsynaptic potentiation in the absence of esterase. See text.

rate constant decreases by a factor of 2.9 between 25° and 15°; at +34 mV the factor is only 2.4. Thus the calculated decay rate constant has a slightly lower Q_{10} at depolarized potentials, as found experimentally by Magleby and Stevens (1972*b*).

POSTSYNAPTIC POTENTIATION IN THE ABSENCE OF ESTERASE Hartzell et al. (1975) showed that the nonlinear dose-response curve and the buffering effect could produce potentiation of both amplitude and duration in postsynaptic responses if the enzymatic hydrolysis is suppressed. Because our equations have radial symmetry, we could not directly simulate the overlapping flanks from two neighboring quanta (Hartzell et al., 1975). Instead, quantal events were calculated for vesicles containing varying numbers of ACh molecules. To allow more room for lateral interactions, we set the cleft radius to 1.5 μm (the standard value is 0.5 μm). Because potentiation would be strongest at the nonlinear start of the dose-response curve, one expects to see marked effects with just a few ACh molecules per vesicle. The calculations bear out these expectations (Fig. 4), and potentiation is clear for vesicle contents of much less than the standard size. For instance, when the quantal size increases from 500 to 2,000 molecules, the calculated response increases by nearly a factor of 10.

Fig. 4 also presents results in agreement with the experimental observation that quantal events with higher peak amplitudes have longer waveforms (Negrete et al., 1972; Fig. 13A of Hartzell et al., 1975). For a detailed comparison with the data, we assume that in the experiment of Hartzell et al. (1975) the channel conductance was 23 pS and the driving force was 75 mV (Dionne and Parsons, 1977). Therefore uniquantal responses of 2 and 6 nA correspond to 1,160 and 3,478 channels, respectively. The observed half-decay times were approximately 3.5 and 5.6 ms for these amplitudes. Calculated responses with these amplitudes have half-decay times of 3.3 and 5.1 ms, in good agreement with the experimental data.

To investigate the importance of cleft geometry in the absence of esterase, we calculated quantal events for the standard number of ACh molecules in a vesicle (10,000) and for various cleft radii (Fig. 5). As the radius increases, potentiation is added at later times and the waveforms have a long, nonexponential "tail" as observed experimentally (Fig. 7A of Hartzell et al., 1975). Peak activation is constant ($\simeq$2,650 channels) for all radii >0.5 μm; and the half-decline time is constant (4.5 ms) for all radii >1.0 μm. Thus in contrast to the simulations with normal esterase, the computed quantal event is strongly influenced by the cleft geometry when the esterase is inhibited; and this fact may underly some of the variability among experimental results obtained with anticholinesterase treatments in different preparations.

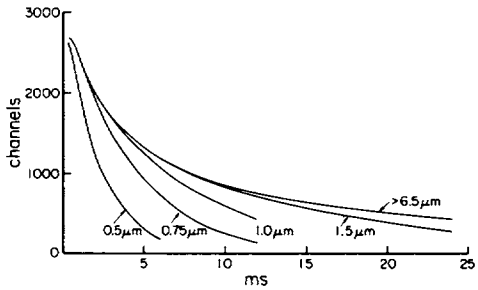

FIGURE 5 Effect of varying cleft radius in the absence of esterase.

DISCUSSION

To the extent that these calculations furnish a good description of the quantal event, both under normal conditions and during the various experimental manipulations, they provide reassurance that one possesses a reasonably complete and self-consistent set of data. Nonetheless we stress that our scheme must remain tentative because we have not seriously explored alternatives to the five fundamental assumptions given in the theory section. Furthermore a number of ancillary assumptions bear discussion here.

(a) The assumptions about acetylcholine-receptor interactions, and about channel activation, derive principally from the voltage-jump relaxation studies of Sheridan and Lester (1977). These studies led to the conclusion that ACh-receptor channels open at a rate that is linear with [ACh] for concentrations in excess of $\simeq$10 μm; at 25°C the constant of proportionality is 2×10^7 $M^{-1}s^{-1}$. We have assumed that this linearity extends to the much higher concentrations that exist locally during the growth phase of the miniature event. An alternative possibility is that the opening rate levels off at high [ACh], possibly because of a rate-limiting conformational change (cf., Magleby and Stevens, 1972*a,b*). Such a scheme receives some support from recent data on the concentration dependence of voltage-jump kinetics (Adams and Sakmann, 1978) and on kinetics with a covalently bound agonist (Lester et al., 1979). If, for instance, the conformational change had a rate constant of 10 ms^{-1}, the computed growth time would be a factor of 1.5–2 longer; and this would agree better with experimental data at 25°C (Gage and McBurney, 1975; Lester et al., 1978). The peak response would be smaller, but this characteristic cannot yet be used as a definitive criterion because it also depends strongly on receptor density and on molecules per vesicle, which are known only approximately.

The specific model used here also predicts that the channel opening rate depends on the square of ACh concentration for [ACh] lower than $\simeq$10 μm = 300 molecules/μm^2. The calculated [ACh] substantially exceeds this value over most of the cleft during the first 500 μs of the standard event (Fig. 2). Therefore, events during this period are not strongly influenced by this assumption. At later times the ACh concentration does drop this low. The number of receptors involved may be estimated in two ways: (1) 300 molecules/μm^2 could open at most 150 channels/μm^2, or 118 receptors within the standard cleft. (2) At 10 μM ACh, the equation for equilibrium activation (Eq. 14 in Sheridan and Lester, 1977) gives 7.9%, or 74 receptors within the synaptic cleft. Other molecular models would make specific predictions about the number of channels activated and about the time-course of activation; but the actual experimental signals might be too small to permit a decision among models.

(b) Transmitter release mechanisms are largely unknown on the time scale (10–100 μs) of interest here. If, for instance, a quantum of transmitter were released over 40–100 μs, rather than instantaneously as assumed, the growth phase would also be longer. A related possibility, considered by Gage and McBurney (1975), is that transmitter crosses the height of the cleft more slowly than the 10 μs or so appropriate to a diffusion coefficient of 3×10^{-6} cm^2/s. Perhaps the cleft has anisotropic diffusion properties.

(c) Another point of uncertainty concerns the enzyme, acetylcholinesterase. We have simply assumed that catalysis proceeds as if the enzyme were free in solution. In fact, however, enzyme molecules are likely to exist in specialized, oligomeric arrays, possibly attached to basement membrane, within the synaptic cleft (Rieger et al., 1973; Dudai et al.,

1973). Although most oligomeric forms of the enzyme have catalytic properties very similar to the basic subunit (Massoulié and Rieger, 1969), esterase function may be greatly influenced by the special molecular environment of the synaptic cleft.

(d) Our calculations are also completely uninformative about the role of specialized structures, such as junctional folds and Schwann cell processes, found at some nicotinic synapses. Because nicotinic synapses all display quantal responses with similar time-course and amplitude, and because the present calculations yield a good description without taking into account these structures at all, one might conclude that these structures do not influence the quantal response directly. The assumed disc-like geometry is certainly an oversimplification, but the calculated standard event is so localized that it remains unaffected by structures located 0.5 μm and further from the release point. Thus it seems, for example, that completely independent quantal events could occur at adjacent "synaptic units" of the frog endplate (Matthews-Bellinger and Salpeter, 1978). The specialized structures may function in the removal of the molecules that appear in the synaptic cleft as a byproduct of the quantal event. Each event produces $\simeq$7,000 acetate and choline ions, an equal number of protons (several orders of magnitude more than the normal number free in the cleft), and $\simeq 1.2 \times 10^6$ K^+ ions ($\simeq$100 times the normal number).

The normal quantal event also seems relatively immune to "off-center" release. If the release point is 0.25 μm, or only 5 vesicle diameters, from 1 edge of an extensive synapse, the results of Table III allow the conclusion that peak activation would be diminished by only 10%.

In conclusion it may be stated that these calculations provide justification and additional confirmation for the following concepts that derive from recent research. When the esterase is active, most receptors near the point of release are activated once by ACh molecules which are then rapidly hydrolyzed when released from receptors. When esterase is inactive, the quantal event spreads radially and its time-course is governed by multiple activation and by buffered diffusion.

We thank D. L. Armstrong, M. E. Krouse, T. L. Rosenberry, M. M. Salpeter, and R. E. Sheridan for helpful discussion.

This work was supported by the Muscular Dystrophy Association of America (postdoctoral fellowship to M.M.N. and grant-in-aid) and by the U.S. National Institutes of Health (Research Career Development Award NS-272 to H.A.L. and grant NS-11756).

Received for publication 30 November 1978 and in revised form 10 February 1979.

REFERENCES

ADAMS, P. R., and B. SAKMANN. 1978. Agonist-triggered end plate channel opening. *Biophys. J.* **21**:53*a*. (Abstr.)

ANDERSON, C. R., and C. F. STEVENS. 1973. Voltage clamp analysis of acetylcholine induced end-plate current fluctuations at frog neuromuscular junction. *J. Physiol. (Lond.).* **235**:655.

ARMSTRONG, D., and H. A. LESTER. 1979. The kinetics of curare action and restricted diffusion within the synaptic cleft. *J. Physiol. (Lond.).* In press.

COLQUHOUN, D. 1975. Mechanisms of drug action at the voluntary muscle end plate. *Annu. Rev. Pharmacol.* **15**:307.

CRANK, J. 1975. The Mathematics of Diffusion. The Clarendon Press, Oxford, England.

DIONNE, V. E. 1976. Characterization of drug iontophoresis with a fast microassay technique. *Biophys. J.* **16**:705.

DIONNE, V. E., and R. L. PARSONS. 1977. Characteristics of the postsynaptic channel at snake neuromuscular junctions. *Biophys. J.* **17**:124*a*. (Abstr.)

DREYER, F., and K. PEPER. 1974. The acetylcholine sensitivity in the vicinity of neuromuscular junction of the frog. *Pfluegers Arch. Eur. J. Physiol.* **348**:273.

DUDAI, Y., M. HERZBERG, and I. SILMAN. 1973. Molecular structures of acetylcholinesterase from electric organ tissue of the electric eel. *Proc. Natl. Acad. Sci. U.S.A.* **70**:2473.

ECCLES, J. C., and J. C. JAEGER. 1958. The relationship between the mode of operation and the dimensions of the junctional regions at synapses and motor end-organs. *Proc. R. Soc. Lond. B. Biol. Sci.* **148**:38.

FERTUCK, H. C., and M. M. SALPETER. 1976. Quantitation of junctional and extrajunctional acetylcholine receptors by electron microscope autoradiography after ^{125}I-α-bungarotoxin binding at mouse neuromuscular junctions. *J. Cell Biol.* **69**:144.

FLETCHER, P., and T. FORRESTER. 1975. The effect of curare on the release of acetylcholine from mammalian motor nerve terminals and an estimate of quantal content. *J. Physiol. (Lond.).* **251**:131.

GAGE, P. W. 1976. Generation of endplate potentials. *Physiol. Rev.* **56**:177.

GAGE, P. W., and R. N. MCBURNEY. 1975. Effects of membrane potential, temperature and neostigmine on the conductance change caused by a quantum of acetylcholine at the toad neuromuscular junction. *J. Physiol. (Lond.).* **244**:385.

GAGE, P. W., and D. VAN HELDEN. 1979. Effects of permeant monovalent cations on end-plate channels. *J. Physiol. (Lond.).* In press.

HARTZELL, H. C., S. W. KUFFLER, and D. YOSHIKAMI. 1975. Post-synaptic potentiation: interaction between quanta of acetylcholine at the skeletal neuromuscular synapse. *J. Physiol. (Lond.).* **251**:427.

HEUSER, J. E., and T. S. REESE. 1973. Evidence for recycling of synaptic vesicle membrane during transmitter release at the frog neuromuscular junction. *J. Cell Biol.* **57**:315.

JAKOPIN, P., and M. KORDAS. 1977. On the role of junctional cholinesterase in determining the time course of the end-plate potential. Appendix. *J. Physiol. (Lond.).* **270**:133.

KATZ, B., and R. MILEDI. 1972. The statistical nature of the acetylcholine potential and its molecular components. *J. Physiol. (Lond.).* **224**:665.

KATZ, B., and R. MILEDI. 1973. The binding of acetylcholine to receptors and its removal from the synaptic cleft. *J. Physiol. (Lond.).* **231**:549.

KORDAS, M. 1972*a*. An attempt at an analysis of the factors determining the time course of the end-plate current. I. The effects of prostigmine and of the ratio of Mg^{2+} to Ca^{2+}. *J. Physiol. (Lond.). 224:317.*

KORDAS, M. 1972*b*. An attempt at an analysis of the factors determining the time course of the end-plate potential. II. Temperature. *J. Physiol. (Lond.).* **224**:333.

KUFFLER, S. W., and D. YOSHIKAMI. 1975. The number of transmitter molecules in a quantum: an estimate from iontophoretic application of acetylcholine at the neuromuscular synapse. *J. Physiol. (Lond.).* **251**:265.

LESTER, H. A. 1970. Postsynaptic action of cobra toxin at the myoneural junction. *Nature (Lond.).* **227**:727.

LESTER, H. A. 1972. Blockade of acetylcholine receptors by cobra toxin: electrophysiological studies. *Mol. Pharmacol.* **8**:623.

LESTER, H. A., D. D. KOBLIN, and R. E. SHERIDAN. 1978. Role of voltage-sensitive receptors in nicotinic transmission. *Biophys. J.* **21**:181.

LESTER, H. A., M. E. KROUSE, M. M. NASS, N. H. WASSERMAN, and B. F. ERLANGER. A covalently bound photoisomerizable agonist at *Electrophorus* electroplaques: equilibria, kinetics, and stoichiometry. *Soc. Neurosci. Symp. Abstr.* In press.

LEVENSON, G. I. P. 1977. Diffusion transfer and monobaths. *In* The Theory of the Photographic Process. T. H. James, editor. 4th edition. Macmillan, Inc., New York. 466–480.

MAGLEBY, K. L., and C. F. STEVENS. 1972*a*. The effect of voltage on the time course of end-plate currents. *J. Physiol. (Lond.).* **223**:151.

MAGLEBY, K. L., and C. F. STEVENS. 1972*b*. A quantitative description of end-plate currents. *J. Physiol. (Lond.).* **223**:173.

MAGLEBY, K. L., and D. A. TERRAR. 1975. Factors affecting the time course of decay of end-plate currents: a possible cooperative action of acetylcholine on receptors at the frog neuromuscular junction. *J. Physiol. (Lond.).* **244**:467.

MASSOULIÉ, J., and F. RIEGER. 1969. l'acétylcholinestérase des organes électriques de Poissons (torpille et gymnote); complexes membranaires. *Eur. J. Biochem.* **11**:441.

MATTHEWS-BELLINGER, J., and M. M. SALPETER. 1978. Distribution of acetylcholine receptors at frog neuromuscular junctions with a discussion of some physiological implications. *J. Physiol. (Lond.).* **279**:197.

NEGRETE, J., J. DEL CASTILLO, I. ESCOBAR, and G. YANKELEVICH. 1972. Correlation between amplitudes and rise times of the miniature endplate potentials in frog muscle. *Int. J. Neurosci.* **4**:1.

NEHER, E., and B. SAKMANN. 1975. Voltage-dependence of drug-induced conductance in frog neuromuscular junction. *Proc. Natl. Acad. Sci. U.S.A.* **72**:2140.

PATRICK, J., S. F. HEINEMAN, J. LINDSTROM, D. SCHUBERT, and J. H. STEINBACH. 1972. Appearance of acetylcholine receptors during differentiation of a myogenic cell line. *Proc. Natl. Acad. Sci. U.S.A.* **69**:2762.

PEPER, K., F. DREYER, C. SANDRI, K. AKERT, and H. MOOR. 1974. Structure and ultrastructure of the frog motor endplate. A freeze-etching study. *Cell Tissue Res.* **149**:437.

RIEGER, F., S. BON, J. MASSOULIÉ, and J. CARTAUD. 1973. Observation par microscopie électronique des formes allongées et globulaires de l'acétylcholinestérase degymnote *(Electrophorus electricus)*. *Eur. J. Biochem.* **34**:539.

ROSENBERRY, T. 1975. Acetylcholinesterase. *In* Advances in Enzymology. **43**:103–218.

ROSENBERRY, T. 1979. Quantitative simulation of endplate currents at neuromuscular junctions based on the reaction of acetylcholine with acetylcholine receptor and acetylcholinesterase. *Biophys. J.* **26**:263.

SHERIDAN, R. E., and H. A. LESTER. 1975. Relaxation measurements on the acetylcholine receptor. *Proc. Natl. Acad. Sci. U.S.A.* **72**:3496.

SHERIDAN, R. E., and H. A. LESTER. 1977. Rates and equilibria at the acetylcholine receptor of *Electrophorus* electroplaques: a study of neurally evoked postsynaptic currents and of voltage-jump relaxations. *J. Gen. Physiol.* **70**:187.

SMITH, G. D. 1965. Numerical Solution of Partial Differential Equations. Oxford University Press, London, England.

STEINBACH, J. H., and C. F. STEVENS. 1976. Neuromuscular transmission. *In* Frog Neurobiology, R. Llinas, and W. Precht, editors. Springer-Verlag GmBH, Berlin, West Germany.

STEVENS, C. F. 1978. Interactions between intrinsic membrane protein and electric field: an approach to studying nerve excitability. *Biophys. J.* **22**:295.

WEBER, M. and J. P. CHANGEUX. 1974. Binding of Naja nigricollis [^{3}H]α-toxin to membrane fragments from *Electrophorus* and *Torpedo* electric organs. I. Binding of the tritiated α-neurotoxin in the absence of effector. *Mol. Pharmacol.* **10**:1.